Patterning Colloidal Films via Evaporative Lithography

Daniel J. Harris,[1] Hua Hu,[2] Jacinta C. Conrad,[1,3] and Jennifer A. Lewis[1,*]

[1]*Department of Materials Science and Engineering and Frederick Seitz Materials Research Laboratory, University of Illinois at Urbana-Champaign, Urbana, Illinois 61801, USA*

[2]*Corporate Engineering Technical Lab, The Procter and Gamble Company, West Chester, Ohio 45069, USA*

[3]*INEST Group Postgraduate Program, Philip Morris USA, Richmond, Virginia 23234, USA*

(Received 19 December 2006; published 5 April 2007)

We investigate evaporative lithography as a route for patterning colloidal films. Films are dried beneath a mask that induces periodic variations between regions of free and hindered evaporation. Direct imaging reveals that particles segregate laterally within the film, as fluid and entrained particles migrate towards regions of higher evaporative flux. The films exhibit remarkable pattern formation that can be regulated by tuning the initial suspension composition, separation distance between the mask and underlying film, and mask geometry.

DOI: 10.1103/PhysRevLett.98.148301 PACS numbers: 82.70.Dd, 47.57.ef, 68.03.Fg

The ability to pattern colloidal films is of growing importance for the fabrication of photonic crystals [1], coatings [2], and metallized ceramic layers [3]. Patterned colloidal assemblies are typically created by exposing colloids to chemically [4,5] or topographically [6–8] modified substrate surfaces. However, such approaches are not easily applied to other classes of soft materials. By contrast, scant attention has been given to patterning routes that rely on controlled particle convection, even though prior studies of freely evaporating droplets [9–12] and films [13,14] have convincingly demonstrated that particles or other soluble species (e.g., DNA) entrained in the liquid phase migrate during drying. For example, when a drying droplet wets the surface and its contact line is pinned, solvent and entrained particles flow to the drop periphery, yielding the familiar ''coffee-ring'' pattern [9]. Recently, it has been shown that more complex patterns form when a concentrated latex film is exposed to periodically varying regions of free and hindered evaporation [15]. In a single experiment, a mask containing a hexagonal array of centimeter-sized holes was placed above a drying suspension, resulting in the formation of a continuous film with raised features. Despite the conceptual simplicity of this approach, herein referred to as evaporative lithography, the observed pattern formation in colloidal films is poorly understood.

In this Letter, we investigate the assembly of unary and binary colloidal films via evaporative lithography through a combination of experiment and finite-element modeling (FEM). We vary the colloid volume fraction, mask design, and separation distance between the mask and underlying film (Fig. 1), and measure the extent of particle segregation using optical, fluorescence, and confocal microscopy. Patterned films are produced with discrete features as small as several microns in height, whose lateral dimensions are approximately equivalent to the hole diameter d_h. We observe a transition from discrete patterned features to continuous patterned films as the colloid volume fraction increases, and show that this transition can be exploited in multicomponent suspensions to preferentially segregate one species in a continuous film of another. We calculate the evaporative landscape above the drying films using FEM to understand the effects of mask design and placement on particle migration. We find that particle segregation becomes negligible when the difference in the evaporation rates between masked and unmasked regions of the drying film approaches that of a freely evaporating film. This transition occurs at a critical value of the scaling parameter h_g/P, where h_g is the initial gap height between the mask and the underlying film and P is the pitch, or center-to-center separation distance between the open features in the mask. Our results provide a fundamental understanding of these important physical parameters, and simultaneously demonstrate the broad applicability of this approach.

Unary colloidal films are produced from aqueous suspensions of silica microspheres with radius $a_\mu = 0.59\ \mu$m. These suspensions are prepared with varying microsphere volume fraction ϕ_μ at pH 7, where the particles are charge stabilized (zeta potential $\zeta_\mu \approx -55$ mV). Binary films are produced from aqueous suspensions of

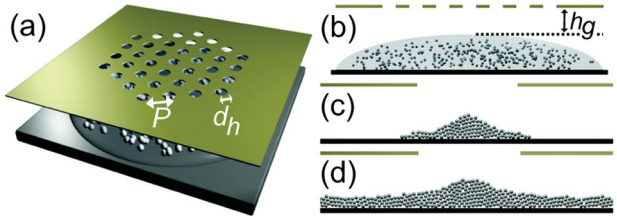

FIG. 1 (color). Schematic presentation of the evaporative lithography process. (a) Top view illustrating the mask design, including the pitch P and hole diameter d_h. (b) Side view of an as-deposited film. Magnified views of (c) a discrete patterned feature prepared from a dilute suspension, and (d) a continuous patterned film prepared from a concentrated suspension.

silica microspheres and fluorescently labeled, sulfonated polystyrene nanoparticles with radius $a_n = 10$ nm. These suspensions are prepared at *p*H 3 with $\phi_\mu = 0.3$ and nanoparticle volume fraction $\phi_n = 10^{-3}$. In this case, the microspheres are negligibly charged ($\zeta_\mu \approx -1$ mV) when suspended alone in solution, but are stabilized by the self-organization of highly charged ($\zeta_n \approx -120$ mV) nanoparticle "halos" around each microsphere when $\phi_n > 10^{-4}$ [16–18]. Films are produced by first depositing a given suspension onto a glass substrate to achieve an initial film height $h_i \approx 100$ μm, and then drying it under a patterned mask. All masks contain a hexagonal array of holes with $d_h = 250$ or 500 μm and $P = 2$, 5, or $10d_h$; h_g is varied between 30 and 1400 μm.

To directly observe particle migration during evaporative lithography, we use fluorescence microscopy to image the flow of fluorescently labeled silica microspheres [19]. We acquire a time-lapse video of a film with $\phi_\mu = 0.005$ that is drying under a mask with $d_h = 250$ μm, $P = 5d_h$, and $h_g \approx 30$ μm [20] and show representative images in Figs. 2(a)–2(c). The image plane resides slightly above the substrate surface, and is centered below an open region in the mask. We calculate the intensity profile across the patterned feature shown in each image, and report this in Fig. 2(d). Initially, the microspheres are evenly distributed throughout the film [Fig. 2(a)] and the intensity profile is flat. As drying proceeds, the microspheres migrate towards the unmasked region leading to a substantial increase in their local concentration [Fig. 2(b)], as reflected by a peak in the intensity profile. Upon further drying, the patterned feature continues to grow [Fig. 2(c)], as indicated by increases in both the height and width of the peak in the intensity profile. Near the end of the drying process, the contrast is further increased by the diminishing concentration of water within the film. We estimate the sedimentation time for a single microsphere (radius $a = 0.5$ μm) within the drying film by dividing h_i by the Stokes velocity $U_0 = 2a^2\Delta\rho g/9\mu$ [21], where $\Delta\rho = 1$ g/mL is the density difference between the microspheres and water, g is the acceleration due to gravity, and $\eta = 0.89$ cP is the fluid viscosity. Even though the total drying time (≈ 120 min) greatly exceeds the sedimentation time (≈ 2 min), nearly all of the particles are nevertheless transported to the unmasked region.

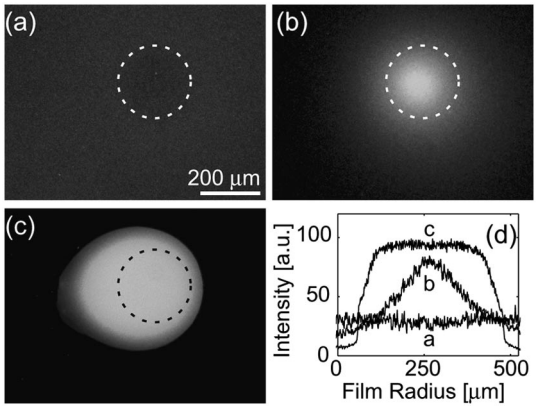

FIG. 2. Fluorescence images of a drying film with $\phi_\mu = 0.005$, $d_h = 250$ μm, $P = 5d_h$, and $h_g \approx 30$ μm as a function of drying time; t: (a) 30 min, (b) 90 min, and (c) 99 min. (d) The intensity profiles versus film radius calculated for (a)–(c). The dashed circle in each image denotes the location of the open feature in the drying mask.

To explore the effects of colloid volume fraction on pattern formation, we dry, image, and measure the height profiles of unary films dried under a fixed mask design. We vary ϕ_μ from 0.005 to 0.3, and fix $d_h = 250$ μm, $P = 5d_h$, and $h_g \approx 30$ μm, and show the optical images in Figs. 3(a)–3(c). Contact-line pinning occurs during film drying, leading to "coffee-ring" formation. However, this feature lies outside the imaged areas and is not shown. The corresponding film height profiles are measured by contact profilometry and shown in Fig. 3(d). When the microsphere suspension is dilute ($\phi_\mu = 0.005$), discrete patterned features form [Fig. 3(a)]; the feature height h_f is ≈ 8 μm and the feature diameter d_f is roughly 400 μm, of the order of d_h. The feature diameter increases with increasing ϕ_μ, as shown in Fig. 3(e). When ϕ_μ exceeds a critical initial microsphere volume fraction ϕ_μ^*, d_f is greater than the pitch and there is a transition from discrete patterned features to continuous patterned films [Fig. 3(b)]. When $\phi_\mu \gg \phi_\mu^*$, thicker films with patterned surfaces are produced [Fig. 3(c)]. To determine ϕ_μ^*, we set $d_f = P$ and equate the total initial microsphere volume within a hexagonal region around each open feature, $V_i = \phi_\mu(P^2\sqrt{3}/2)h_i$, to the final microsphere volume within

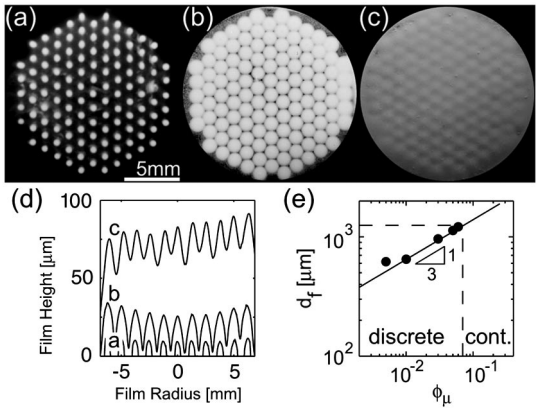

FIG. 3. Optical images of films prepared from colloidal suspensions with $\phi_\mu =$ (a) 0.005, (b) 0.1, and (c) 0.3, and (d) the corresponding height profiles. (e) The feature diameter d_f as a function of ϕ_μ. The solid line has slope $\frac{1}{3}$. The horizontal dashed line denotes $d_f = P$ and the vertical dashed line denotes the critical microsphere volume fraction at the transition from discrete to continuous patterned films. Each film was dried under a mask with $d_h = 250$ μm, $P = 5d_h$, and $h_g \approx 30$ μm.

each cap-shaped patterned feature, $V_f = \phi_f \pi h_f(\frac{3}{4}d_f^2 + h_f^2)/6$. Here, we assume $\phi_f = 0.64$, the random close-packed volume fraction for monodisperse spheres, and take $h_f/d_f \approx 0.02$, based on experimental measurements. Both the mask design and evaporation rate affect the aspect ratio of the patterned features. For example, discrete patterned features dried under masks with smaller d_h/P have a smaller aspect ratio. We calculate $\phi_\mu^* \approx \pi\phi_f P/200\sqrt{3}h_i \approx 0.07$, in good agreement with our experimental observations [Fig. 3(e)].

To quantify the effects of mask design and placement on pattern formation, we measure the difference between the average maximum and minimum film heights, $\Delta\bar{h} = \bar{h}_{\max} - \bar{h}_{\min}$, as a function of h_g/P for a series of continuous films. We prepare films with fixed $\phi_\mu = 0.2$, and dry them under masks with varying d_h, P, and h_g. When $h_g/P < 0.3$, large variations in film height are observed [Fig. 4(a)]. For $h_g/P \geq 0.3$, the variations in film height are negligible, indicating that little particle segregation occurs. For fixed h_g/P, continuous films dried under masks with larger P exhibit greater height variations, because there is a greater volume of fluid and entrained particles drawn from the unmasked regions surrounding each open feature.

Our observations provide strong evidence that the mask design and placement significantly influence the evaporative landscape above the drying film. To quantify these effects, we calculate the evaporative flux J across the film surface using FEM analysis [22]. As an example, the calculated evaporative flux as a function of film radius for a film drying under a mask with $d_h = 250$ μm, $P = 5d_h$, and $h_g \approx 150$ μm is shown in the inset of Fig. 4(b). The FEM analysis reveals that the maximum evaporative flux $J_{\max}$ occurs under the open regions, whereas the minimum evaporative flux $J_{\min}$ approaches zero under the masked regions of the drying film. Although fluid evaporation is higher in the open regions, surface tension acts to keeps the drying film flat. Therefore, fluid must flow toward the evaporating regions to compensate for the fluid loss and the entrained particles accumulate beneath the open regions. We summarize our findings by plotting the difference in the evaporative flux $\Delta J = J_{\max} - J_{\min}$, normalized by the evaporative flux of a freely evaporating film J_{free}, as a function of h_g/P for films dried under masks with a broad range of d_h, P, and h_g values [Fig. 4(b)]. These data are fit by a master curve, $\Delta J/J_{\text{free}} \propto \exp(-\alpha h_g/P)$, with $\alpha = 6.06 \pm 0.29$. This indicates that when either h_g is small or P is large, evaporation is strongly suppressed under the masked regions. As h_g is increased or P is decreased, the ability of the mask to locally hinder evaporation diminishes, leading to a dramatic decrease in ΔJ. At the critical value of $h_g/P = 0.3$ identified experimentally, FEM analysis predicts $\Delta J/J_{\text{free}} \approx 1$ [Fig. 4(b)]. Thus, $\Delta J/J_{\text{free}}$ must exceed unity to induce significant particle segregation.

To determine the minimum feature size that can be patterned, we compare the diffusion time to the convection time by calculating the Peclet number $\text{Pe} = u_x(P - d_h)/2D_0$. Here, u_x is the horizontal particle velocity, $(P - d_h)/2$ is the distance from the center of a masked region to a hole edge, and D_0 is the Stokes-Einstein diffusion coefficient. We relate the vertical velocity $u_z = J_{\text{mean}}/\rho$, where J_{mean} is the average evaporative flux of a masked film and ρ is the fluid density, to the horizontal velocity $u_x = u_z P/2h_i$ via the lubrication approximation. At constant temperature and humidity, we measure J_{mean} for films dried under masks of varying design and J_{free}, and find that $J_{\text{mean}} = J_{\text{free}}(d_h/P)$, yielding $\text{Pe} = J_{\text{free}} d_h(P - d_h)/4\rho D_0 h_i$. When $\text{Pe} > 1$, convection dominates and pattern formation is observed. When $\text{Pe} < 1$, diffusion dominates, thereby hin-

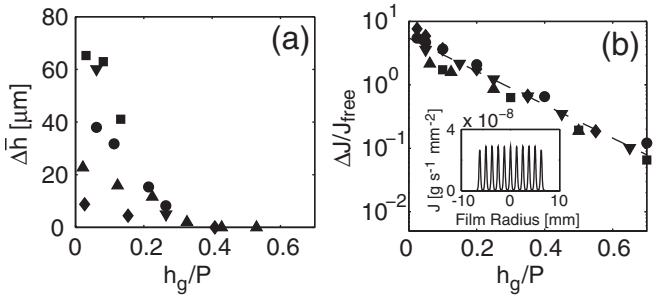

FIG. 4. (a) Measured film height variations versus h_g/P. (b) Calculated variations in the evaporative flux profile normalized by the flux of a freely evaporating film versus h_g/P. *Mask parameters*: ■, $d_h = 500$ μm, $P = 10d_h$; ▼, $d_h = 500$ μm, $P = 5d_{\text{hole}}$; ●, $d_h = 250$ μm, $P = 10d_h$; ▲, $d_h = 250$ μm, $P = 5d_h$; ◆, $d_h = 500$ μm, $P = 2d_h$. The dashed line in (b) is a fit to the data and the inset shows the evaporation profile of a film dried under a mask with $d_h = 250$ μm, $P = 5d_h$, and $h_g \approx 150$ μm.

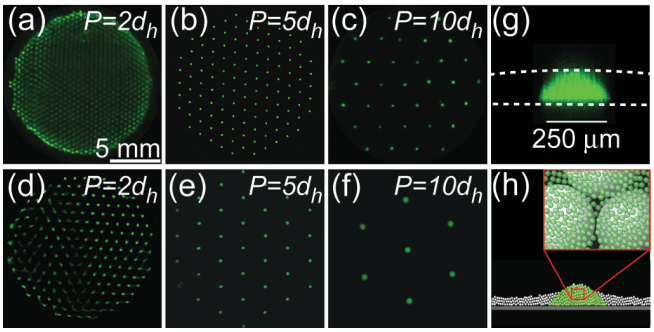

FIG. 5 (color). Fluorescence images of patterned microsphere-nanoparticle films dried under masks with (a)–(c) $d_h = 250$ μm and (d)–(f) 500 μm and varying P. (g) Confocal micrograph (x-z plane) of a single feature in the binary film shown in (b). The dashed white line indicates the approximate height profile of the continuous film. (h) Schematic illustrating the fluorescent nanoparticles segregated in the microsphere network. Note: Images (a)–(f) are constructed by tiling multiple images; only the nanoparticles are imaged.

dering pattern formation. For a film dried under a mask with $d_h = 25\ \mu$m and $P = 250\ \mu$m, we calculate Pe ≈ 1, and observe very little particle segregation. However, smaller features can be patterned either by increasing J_{mean}, which is a function of d_h, P, temperature, and humidity, or decreasing D_0.

To explore evaporative lithography of multicomponent systems, films are formed from binary microsphere-nanoparticle suspensions ($\phi_\mu = 0.3$, $\phi_n = 10^{-3}$) and dried under masks of varying d_h and P, at constant $h_g \approx 30\ \mu$m. Under these conditions, the microspheres consolidate to form a continuous patterned film whose surface topography is nearly identical to that shown in Fig. 3(c), while the fluorescently labeled nanoparticles segregate to the unmasked regions, yielding discretely patterned features [Figs. 5(a)–5(f)] within the microsphere film. We directly image the nanoparticle distribution within a single patterned feature, prepared under the same conditions as the film shown in Fig. 5(c), using confocal microscopy. To reduce scattering from the nonfluorescent silica microspheres, the film is imbibed with a dimethyl-sulfoxide/water solution that matches their refractive index. The nanoparticles are localized in a region with lateral dimensions $\approx d_h$ and height similar to that of the continuous microsphere film, giving an aspect ratio $h_f/d_f \approx 0.3$, as shown in the confocal image (x-z plane) in Fig. 5(g). By contrast, the aspect ratio of discrete patterned features in films prepared from dilute unary suspensions ($\phi_\mu = 0.005$) is an order of magnitude smaller [Fig. 3(d)].

This difference in film structure indicates that the morphological evolution of binary films patterned by evaporative lithography is more complicated than that observed for unary films. Initially, the silica microspheres and polystyrene nanoparticles are transported to the evaporating regions by particle convection. Given their higher initial volume fraction, the microspheres quickly consolidate into a close-packed network that contains interstitial pores with a radius $a_p \approx 0.15 a_\mu$. The nanoparticles, however, remain entrained in the liquid and are readily transported through the porous microsphere network, since $a_n \ll a_p$. As the drying front recedes into the microsphere network, capillary tension at the liquid menisci creates a pressure gradient, $P_c = -2\gamma_{lv}/a_p$, that further influences nanoparticle segregation, where γ_{lv} is the liquid-vapor surface tension. Using the measured surface tension of 27 mN/m, the calculated pressure drop is ≈ -6 atm. This capillary pressure provides an additional driving force that enhances nanoparticle segregation to the unmasked regions of the binary film.

In summary, we have investigated a novel assembly route for patterning colloidal films, known as evaporative lithography. By modifying the evaporation profile, both discrete patterned features and continuous patterned films are assembled from unary and binary colloidal suspensions. The evaporation profile, resulting particle segregation, and minimum feature size are controlled by the mask design, placement, colloid volume fraction, and size. This technique has several advantages over other assembly routes, including its simplicity, the ability to control particle deposition without substrate modification, and the capacity to guide the distribution of multiple species simultaneously during drying. Thus, evaporative lithography offers a promising new avenue for patterning a broad array of soft materials, including colloids, polymers, and biomolecules.

This material is based on work supported by the U.S. Department of Energy, Division of Materials Sciences under Contract No. DEFG-02-91ER45439, through the Frederick Seitz Materials Research Laboratory. We thank A. Mohraz and A. Chan for useful discussions. J. C. C. is supported through the Interdisciplinary Network of Emerging Science and Technologies (INEST).

*Electronic address: jalewis@uiuc.edu

[1] Y. Vlasov *et al.*, Nature (London) **414**, 289 (2001).
[2] J. Sun, W. Gerberich, and L. Francis, J. Polym. Sci., Part B: Polym. Phys. **41**, 1744 (2003).
[3] Y. Masuda *et al.*, J. Colloid Interface Sci. **263**, 190 (2003).
[4] J. Aizenberg, P. V. Braun, and P. Wiltzius, Phys. Rev. Lett. **84**, 2997 (2000).
[5] H. Zheng *et al.*, Adv. Mater. **14**, 569 (2002).
[6] W. Lee *et al.*, Langmuir **20**, 5262 (2004).
[7] A. van Blaaderen, R. Ruel, and P. Wiltzius, Nature (London) **385**, 321 (1997).
[8] K. H. Lin *et al.*, Phys. Rev. Lett. **85**, 1770 (2000).
[9] R. Deegan *et al.*, Nature (London) **389**, 827 (1997).
[10] H. Hu and R. G. Larson, Langmuir **21**, 3963 (2005).
[11] I. I. Smalyukh *et al.*, Phys. Rev. Lett. **96**, 177801 (2006).
[12] J. Jing *et al.*, Proc. Natl. Acad. Sci. U.S.A. **95**, 8046 (1998).
[13] J. J. Guo and J. A. Lewis, J. Am. Ceram. Soc. **82**, 2345 (1999).
[14] R. C. Chiu and M. J. Cima, J. Am. Ceram. Soc. **76**, 2769 (1993).
[15] A. F. Routh and W. B. Russel, AIChE J. **44**, 2088 (1998).
[16] V. Tohver *et al.*, Proc. Natl. Acad. Sci. U.S.A. **98**, 8950 (2001).
[17] A. T. Chan and J. A. Lewis, Langmuir **21**, 8576 (2005).
[18] J. Liu and E. Luijten, Phys. Rev. Lett. **93**, 247802 (2004).
[19] N. A. M. Verhaegh and A. van Blaaderen, Langmuir **10**, 1427 (1994).
[20] See EPAPS Document No. E-PRLTAO-98-088714 for a time-lapse video of the drying process. For more information on EPAPS, see http://www.aip.org/pubservs/epaps.html.
[21] W. B. Russel, D. A. Saville, and W. R. Schowalter, *Colloidal Dispersions* (Cambridge University Press, Cambridge, U.K., 1989).
[22] H. Hu and R. G. Larson, J. Phys. Chem. B **110**, 7090 (2006).